hydrology

MDPI

Article

Study on Characteristics of Floating Ice Accumulation and Entrainment Safety Thresholds Upstream of Sluice Gates Based on Model Tests and Logistic Regression

Suming Li [1,2,3], Chao Li [1,2,3,*], Huiping Hou [1,2,3], Shiang Zhang [1,2,3] and Xizhi Lv [4]

[1] College of Water Conservancy and Civil Engineering, Inner Mongolia Agricultural University, Hohhot 010018, China; lctd-l@emails.imau.edu.cn (S.L.); 2025202060044@emails.imau.edu.cn (H.H.); 13061531537@emails.imau.edu.cn (S.Z.)
[2] State Key Laboratory of Water Engineering Ecology and Environment in Arid Area, Inner Mongolia Agricultural University, Hohhot 010018, China
[3] Autonomous Region Collaborative Innovation Center for Integrated Management of Water Resources and Water Environment in the Inner Mongolia Reaches of the Yellow River, Hohhot 010018, China
[4] Yellow River Institute of Hydraulic Research, Key Laboratory of the Loess Plateau Soil Erosion and Water Loss Process and Control of Ministry of Water Resources, Zhengzhou 450003, China; nihulvxizhi@163.com
* Correspondence: nmndlc@imau.edu.cn

Abstract

In the complex flow fields of channels affected by sluice gates and bridge piers, winter ice transport, accumulation characteristics upstream of the gate, and the determination of entrainment thresholds are crucial for the safe operation of hydraulic projects. In this study, ice transport experiments were conducted with and without bridge piers upstream of the gate to analyze the key factors governing the transport process and accumulation morphology of floating ice. Four machine learning models were evaluated and compared to identify the optimal model for predicting the motion state of floating ice. Based on this optimal model, the discriminant conditions for ice entrainment under both pier configurations were proposed. The results indicate that, driven by incoming hydraulic parameters, gate boundary conditions, and ice discharge, the upstream floating ice undergoes a progressive evolution: "flat accumulation → "∇"-shaped accumulation → wedge-shaped accumulation → passing through the gate (entrainment)". Compared to the GBDT, RF, and SVM models, the LR model achieves higher and more stable accuracy, precision, recall, and F1 scores under configurations without and with bridge piers. With AUC values reaching 0.993 and 0.997, respectively, this model demonstrates optimal comprehensive performance in classifying whether floating ice passes through the gate. Furthermore, based on the LR model, explicit algebraic formulas for the critical entrainment thresholds were constructed. Under the experimental conditions, the critical threshold intervals for the relative gate opening (e/H) are [0.170, 0.182] without piers and [0.142, 0.155] with piers. This study provides a solid theoretical foundation and technical support for ice-prevention operations and gate dispatching in cold-region hydraulic engineering under submerged outflow conditions.

Keywords: sluice gate; bridge pier; ice floe entrainment; logistic regression; safety threshold

Check for updates

Academic Editor: Michael Nones

Received: 1 February 2026
Revised: 5 March 2026
Accepted: 5 March 2026
Published: 6 March 2026

Copyright: © 2026 by the authors. Licensee MDPI, Basel, Switzerland. This article is an open access article distributed under the terms and conditions of the Creative Commons Attribution (CC BY) license.

1. Introduction

In cold-region rivers during winter, ice jams formed by floating ice can severely reduce the flow cross-section, obstructing downstream discharge and causing a rapid rise in

upstream water levels, which may trigger ice-jam floods [1,2]. Sluice gates and bridges are common hydraulic structures in river systems, and their operational stability is critical to river safety and functional efficiency [3]. During winter water diversion operations in cold regions, hydrodynamic forces make floating ice highly prone to entering gate slots, which can paralyze the regulation functions of the gates. Furthermore, once floating ice submerges and passes through the gates (entrainment), it may accumulate downstream, disrupting normal water conveyance [4]. The presence of bridge piers upstream of a sluice gate not only significantly alters the local hydraulic characteristics but also interferes with the normal transport and freeze-up processes of floating ice. Localized ice blockages may form near the gates and piers, thereby exacerbating the risks of ice entrainment and jam formation [5]. Therefore, an in-depth investigation into the accumulation characteristics and submersion mechanisms of floating ice under the combined effects of sluice gates and bridge piers holds substantial engineering and practical significance. It is vital for ensuring the safe operation of winter water conveyance projects and for optimizing ice-prevention and disaster-mitigation dispatching strategies. Driven by these critical engineering demands, scholars have continuously investigated the motion dynamics of floating ice upstream of sluice gates and bridge piers.

Early studies primarily relied on physical model tests to investigate the critical hydraulic conditions governing the transport and accumulation of floating ice near sluice gates and bridge piers. Through dimensional analysis and simplified moment analysis of idealized ice blocks, Ashton identified that the key controlling parameter for the critical condition of ice entrainment at the leading edge of an ice cover is a thickness-dependent Froude number. By reanalyzing field measurement data of ice transport under submerged gate outflow, Ashton further pointed out the distinct formation conditions and parameter calculation methods for narrow versus wide ice jams [6,7]. The transport and accumulation processes of floating ice upstream of a gate are jointly governed by the approach hydraulic conditions and the gate opening. Consequently, the critical flow velocity and Froude number required for floating ice to pass through the gate vary under different gate openings [8,9]. Using real-ice hydrodynamic experiments in an inverted siphon, Fu et al. [10,11] simulated the accumulation and evolution processes of ice blocks upstream of the siphon inlet under various hydraulic conditions. They derived the relationships among relevant hydraulic parameters for the safe, jam-free operation of the inverted siphon and proposed formulas for calculating ice jam thickness along with its hydraulically controlled critical conditions. Furthermore, the presence of bridge piers in a river channel increases the supporting force exerted on ice jams, thereby altering the formation dynamics of ice jams or ice dams compared to natural channel conditions [12]. Using dimensional and regression analyses, scholars have established empirical equations for the critical Froude number describing floating ice passing through pier cross-sections, and defined the critical concentration thresholds for the formation of ice covers and ice jams [13–18]. Advances in computational power have driven the diversification of research methods, with numerical simulations and intelligent algorithms beginning to play crucial roles in solving complex hydraulic problems. In terms of numerical simulation, the Discrete Element Method (DEM) has been widely applied to simulate the dynamic accumulation processes of ice layers around bridge piers. Coupled with hydrodynamic modeling, these simulations have revealed the nonlinear influence mechanisms of sill placement, gate opening, and discharge on vortex flow fields and discharge capacity [19–21]. In recent years, machine learning (ML) methods have become a research hotspot, primarily due to their core advantage of capturing complex nonlinear relationships within data. Algorithms such as Artificial Neural Networks (ANNs), Support Vector Machine (SVM), and K-Nearest Neighbor (KNN) have been utilized to construct prediction models for the discharge coefficients of sluice

gates, evaluating the sensitivity of parameters including upstream and downstream water levels as well as gate openings [22–24]. Liang et al. [25,26] further proposed a discriminant model for ice transport and accumulation upstream of a channel gate based on Principal Component Analysis (PCA) and SVM, identifying the upstream and exit Froude numbers as the primary controlling factors. Despite these advancements, existing studies have predominantly focused on single hydraulic structures, such as isolated sluice gates or bridge piers. The complex hydraulic characteristics under the coupled effects of sluice gates and bridge piers, as well as their influence mechanisms on the transport and accumulation of floating ice, remain to be thoroughly investigated. Furthermore, although existing machine learning models have improved prediction accuracy, their inherent "black-box" nature makes it difficult to directly apply their quantitative results to engineering dispatch and decision-making.

In this study, physical experiments on ice transport were conducted under configurations both with and without bridge piers upstream of a sluice gate. The key factors governing the transport processes and accumulation morphology of the floating ice were systematically analyzed. Furthermore, four machine learning models were evaluated and compared to identify the optimal model for predicting the motion state of the floating ice. Based on the selected optimal model, explicit discriminant conditions for ice passing through the gate (entrainment) under both pier configurations were proposed. The findings of this research provide a solid theoretical foundation and technical support for the safe operation and scientific dispatch of sluice gates during winter.

2. Experimental Design and Research Methodology

2.1. Experimental Setup

The model experiments were conducted in a straight-walled flume regulated by a sluice gate at the State Key Laboratory of Water Engineering Ecology and Environment in Arid Area. The structural layout of the experimental model is shown in Figure 1. The experimental system (provided by Beijing Precision Wave instrument Co., Ltd., Beijing, China) primarily consists of four components: an independent water supply circulation system, an ice feeder, the main flume body, and a measurement and control system. An ultrasonic flowmeter conceptually divides the flume into an upstream and a downstream section. The upstream section is 12.6 m long, 0.5 m wide, and 0.7 m high, containing 21 cross-sections with a spacing of 0.6 m. The downstream section is 1.6 m long, 1.0 m wide, and 0.9 m high, containing two cross-sections with a spacing of 0.8 m. A steel flat gate is installed at cross-section 17, measuring 1.5 m in height, 0.5 m in width, and 0.03 m in thickness. Influenced by a triangular weir at downstream cross-section 22, the tailwater depth (h_t) in the flume is greater than the conjugate depth of the contracted water depth (h_c) downstream of the gate, resulting in a submerged outflow condition (see Figure 2). To analyze the combined effects of the bridge piers and the sluice gate on the state of floating ice, three acrylic tubes with a diameter of 0.02 m were fixed 0.45 m upstream of the gate to simulate bridge piers (see Figure 3). Electromagnetic flowmeters with an accuracy of ±0.5% are installed in the inlet and outlet pipes, respectively, and an ultrasonic flowmeter with an accuracy of ±2% is deployed 1.8 m downstream of the gate. The ice feeder is located at cross-section 3. Radar flowmeters (±3% accuracy) and radar water level gauges (±1 mm accuracy) are installed 1.2 m downstream of the ice feeder and 1.8 m upstream of the gate, respectively, ensuring the real-time and accurate acquisition of flow velocity, discharge, and water level data. The study is based on an idealized exploratory physical model design. This approach aims to circumvent the experimental noise caused by the heterogeneity in the size, shape, and strength of natural floating ice and bridge piers within the complex flow fields formed by the gate–pier coupling. It allows for the precise isolation of the

hydrodynamic driving mechanisms behind ice entrainment, thereby ensuring experimental controllability and establishing a robust physical baseline [27,28]. Paraffin wax was selected to fabricate the model floating ice, with individual blocks measuring 0.02 × 0.02 × 0.01 m (length × width × thickness). The density of the paraffin blocks is 917 kg/m^3, closely approximating that of natural ice [25]. A total of 4800 model ice blocks were released during the experiment, yielding a cumulative volume (*Vol*) of 0.0192 m^3.

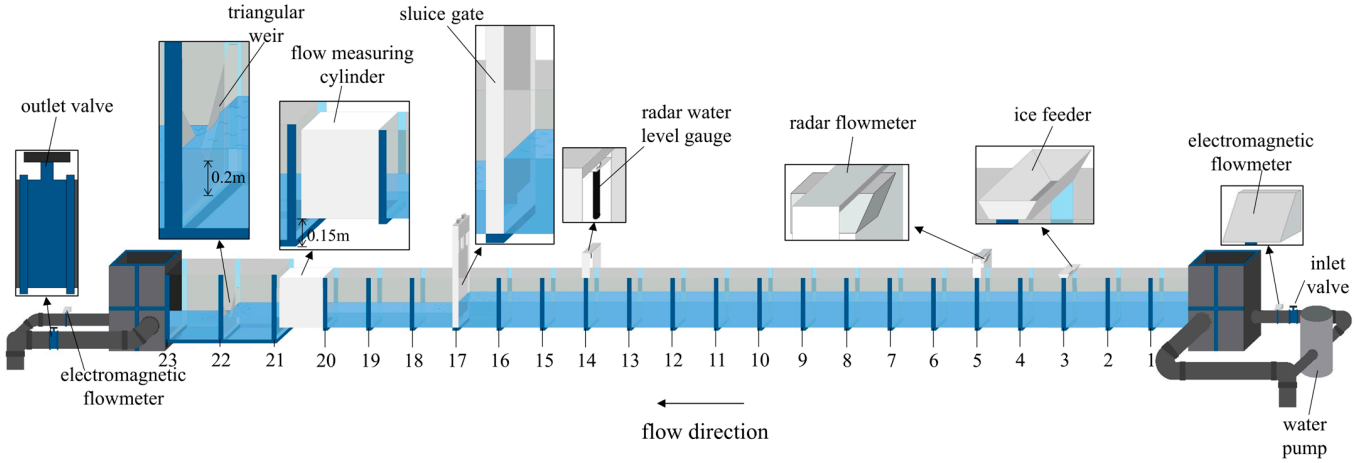


Figure 1. Schematic diagram of the physical experimental model structure.

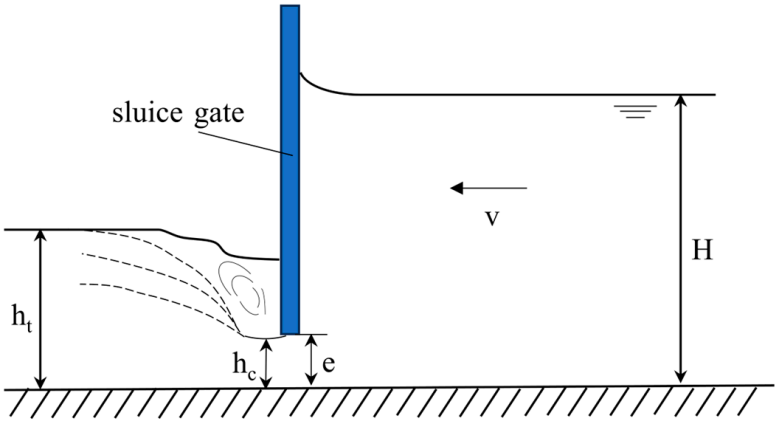


Figure 2. Schematic of flow through the sluice gate under submerged discharge.

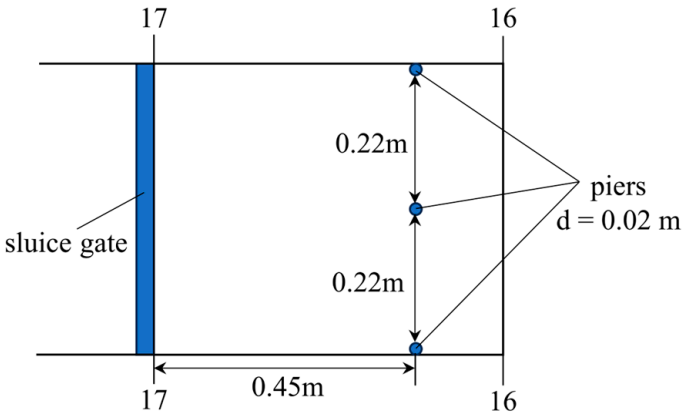


Figure 3. Top view of the gate–piers layout.

2.2. Experimental Scheme

This study is based on generalized physical flume experiments, aiming to reveal the core hydrodynamic mechanisms governing the accumulation and entrainment of floating ice upstream of a sluice gate. The design of the experimental conditions is detailed in Table 1. The experiments were conducted under two configurations: without and with bridge piers. For both configurations, the gate opening (e) was set to 0.045 m, 0.050 m, and 0.055 m. During the experiments, the discharge was regulated using an inlet valve. The flow within the circulating flume was deemed to have reached a steady state—marking the commencement of each experimental trial—when the relative deviation of the discharge measured by flowmeters at all monitoring points was $\leq$4%, and the water level fluctuation remained $\leq$2 mm [29]. An incremental ice-feeding approach was employed to investigate the critical conditions for ice entrainment through the gate. Each incremental batch consisted of 1600 model ice blocks, defining a single sub-condition, with a maximum of three feeding batches per trial. Following each ice release, the motion and accumulation morphology of the floating ice were continuously observed. Once the upstream ice accumulation stabilized, its thickness and length, along with local hydraulic characteristics such as water depth and flow velocity, were systematically measured. If no ice entrained through the gate, the current discharge and gate opening were maintained, and the next batch of ice was released, followed by a repetition of the aforementioned observation and measurement procedures. If no ice entrainment occurred after three consecutive feedings, the final stable data were recorded, and the current trial was terminated. Subsequently, the gate opening or discharge was adjusted to initiate the next set of experiments, and the entire experimental procedure was repeated.

Table 1. Design of experimental conditions.

Case	e (m)	Q (m^3/s)	Number
without piers	0.045	0.0134–0.0241	58
	0.050	0.0167–0.0331	56
	0.055	0.0199–0.0360	51
with piers	0.045	0.0187–0.0325	65
	0.050	0.0223–0.0367	51
	0.055	0.0238–0.0397	48

2.3. Machine Learning Models

Determining whether floating ice passes through a sluice gate is a typical binary classification problem. In this study, four distinct types of machine learning models—Gradient Boosting Decision Tree (GBDT), Random Forest (RF), Support Vector Machine (SVM), and Logistic Regression (LR)—were selected to classify the motion state of the ice (i.e., entrainment or accumulation). Among them, GBDT is a robust ensemble algorithm based on the boosting strategy. It advances training in a serial iterative manner, constructing a new weak classifier at each step to fit the residuals of the preceding models [30]. This mechanism, which continuously reduces the loss function along the gradient direction, enables GBDT to deeply mine data features and typically achieve higher prediction accuracy than single models. RF is an ensemble learning algorithm based on the bagging strategy. Unlike the serial iterative mechanism of GBDT, RF performs parallel computation by constructing multiple independent decision trees and employs a majority voting mechanism to determine the final classification result. By introducing a dual mechanism of sample and feature perturbations, this algorithm significantly reduces model variance, demonstrating strong robustness when dealing with noisy experimental data [31]. SVM is a binary classification model based on the principle of structural risk minimization, achieving classification by

finding the maximum-margin hyperplane. For non-linearly separable data, this study introduces the Radial Basis Function (RBF) kernel to map the original low-dimensional features into a high-dimensional feature space, thereby accurately capturing complex non-linear boundaries [32]. LR is a generalized linear model that uses the Sigmoid function to map the linearly weighted combination of various physical variables to the probability of an event occurring. It yields the contribution weights of each physical variable to the result, offering exceptionally strong physical interpretability [33]. Collectively, these four models cross-validate the data separability and the complexity of the ice–water coupled physical laws from multiple dimensions, including linear, non-linear, and ensemble learning approaches. The parameter settings for the models are detailed in Table 2.

Table 2. The parameter settings for GBDT, RF, SVM, and LR models.

Model	Parameter	Assignment
GBDT	n_estimators	300
	max_depth	5
	random_state	42
	learning rate	0.1
RF	n_estimators	200
	max_depth	8
	random_state	42
	criterion	gini
SVM	random_state	42
	probability	true
	gamma	scale
	kernel	rbf
	C	1.0
LR	random_state	42
	penalty	l2
	solver	lbfgs
	C	1.0

To evaluate the predictive performance of different algorithms regarding the motion state of ice floes, this study selected accuracy, precision, recall, and F1-Score as evaluation metrics.

Recall is defined as the ratio of the number of samples correctly predicted as positive to the total number of actual positive samples. The formula is expressed as:

$$Recall = \frac{TP}{TP + FN} \tag{1}$$

where TP represents true positives, referring to samples predicted as positive that are actually positive; FN represents false negatives, referring to samples predicted as negative that are actually positive.

Accuracy represents the proportion of correctly classified samples relative to the total number of samples. The formula is:

$$Accuracy = \frac{TP + TN}{TP + TN + FP + FN} \tag{2}$$

where FP represents false positives, referring to samples predicted as positive that are actually negative; TN represents true negatives, referring to samples predicted as negative that are actually negative.

Precision is defined as the proportion of actual positive samples among all samples predicted as positive by the model. The formula is:

$$Precision = \frac{TP}{TP + FP} \tag{3}$$

The F1-Score is the harmonic mean of precision and recall. The formula is:

$$F1 = \frac{2 \times Recall \times Precision}{Recall + Precision} \tag{4}$$

3. Results

3.1. Experimental Results and Analysis

The experimental results indicate that, regardless of the presence of bridge piers, the motion state of floating ice upstream of the sluice gate exhibits three distinct phases: flat accumulation extending upstream, balanced stable accumulation upstream of the gate, and entrainment through the gate. Figures 4 and 5 illustrate the accumulation morphologies of floating ice upstream of the gate without and with bridge piers, respectively. It can be observed that under weak initial hydraulic conditions, the hydrodynamic drag force dominates the horizontal motion of the floating ice, while buoyancy and gravity are in equilibrium. Without significant compression between the ice blocks, the floating ice forms a flat accumulation extending upstream, with no ice entrained through the gate. The maximum length of this flat accumulation reached 1.673 m without piers and 1.527 m with piers. As the hydraulic conditions strengthen or the ice discharge increases, ice blocks begin to entrain at the leading edge of the ice cover and are transported to its bottom, forming a "∇"-shaped accumulation. Provided the hydraulic conditions and ice discharge remain constant, this morphology remains stable. The maximum ice thickness at the thickest part of this accumulation was 0.166 m without piers and 0.147 m with piers. With a further increase in discharge or ice feeding, the accumulation of entrained ice causes the thickness at the center of the "∇"-shaped accumulation to continuously increase. This reduces the local flow cross-section and intensifies the hydrodynamic forces, shifting the accumulation of entrained ice closer to the sluice gate. Simultaneously, driven by the flow-induced compaction (shoving) effect, a stable wedge-shaped accumulation is ultimately formed. The maximum ice thickness at the thickest part of the wedge was 0.163 m without piers and 0.152 m with piers. Once the wedge-shaped accumulation reaches a critical threshold, the entrained ice blocks pass through the gate and are transported downstream. Concurrently, under the combined effects of the upstream boundary conditions, gate opening, discharge, and outflow type, vertical-axis vortices may emerge near the gate slots on both sides. These vortices can draw the surrounding floating ice in and carry it through the gate [21]. However, as floating ice accumulates upstream of the gate, it occupies the local flow space, disrupting the hydraulic conditions necessary for vortex formation, which leads to the dissipation of the vertical-axis vortices [26]. Figure 6 presents a schematic diagram of the ice entrainment and accumulation process upstream of the gate, demonstrating a progressive evolutionary sequence: "flat accumulation (D) → '∇'-shaped (E) → wedge-shaped (F) → passing through the gate (entrainment)."

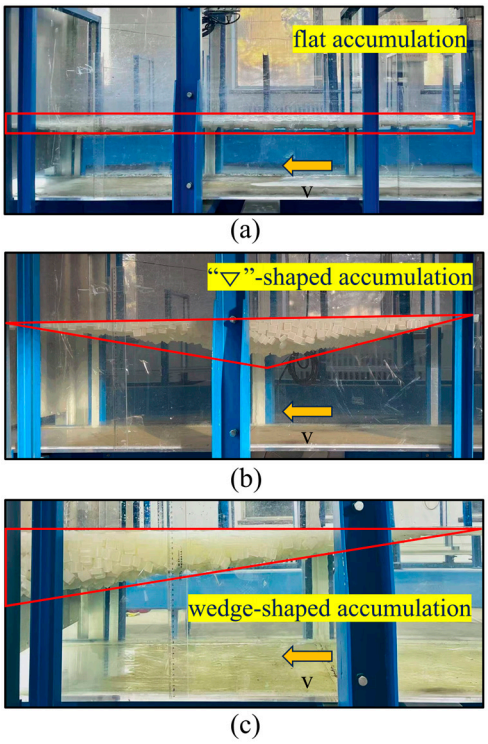


Figure 4. Typical accumulation morphology of ice floes upstream of the sluice gate without bridge piers. ((**a**) flat accumulation extending upstream; (**b**) "∇"-shaped ice accumulation; (**c**) wedge-shaped ice accumulation).

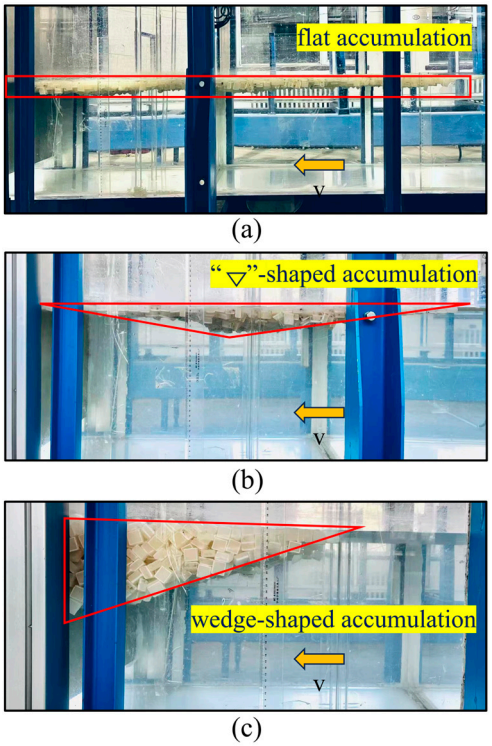


Figure 5. Typical accumulation morphology of ice floes upstream of the sluice gate with bridge piers. ((**a**) flat accumulation extending upstream; (**b**) "∇"-shaped ice accumulation; (**c**) wedge-shaped ice accumulation).

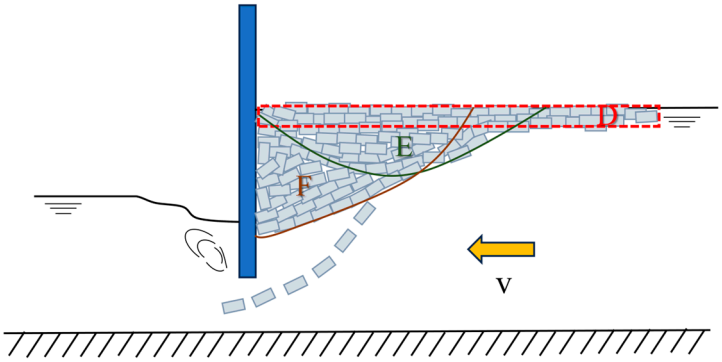


Figure 6. Schematic diagram of the ice entrainment and accumulation process upstream of the sluice gate.

The motion state of ice floes upstream of the sluice gate is influenced by initial hydraulic conditions and gate boundary conditions. Figure 7 presents the relationship between the Froude number (Fr) and the gate opening-to-depth ratio (e/H) under different ice volumes (Vol) with and without bridge piers. As shown in the figure, the probability of ice floes passing through the sluice gate is positively correlated with Fr and e/H; larger values of Fr and e/H indicate a higher likelihood of ice submersion and passage through the gate. Compared to the case without bridge piers, the values of Fr and e/H required for ice floes to pass through the gate are smaller when bridge piers are present. Under otherwise constant conditions, as Vol increases, some ice floes transition from accumulating in front of the gate to passing through it. Figure 8 shows the relationship between the ice Froude number (Fr_b) and the ice thickness-to-depth ratio (t_i/H) under different gate openings (e) with and without bridge piers. Here $Fr_b = v_b/[gt_i(1-\rho_i/\rho)]^{0.5}$, v_b represents the ice velocity, taken as the average surface flow velocity [26]; ρ and ρ_i are the densities of water and ice, respectively; and t_i is the thickness of a single ice block. The probability of ice floes passing through the gate is negatively correlated with Fr_b and positively correlated with t_i/H. Compared to the case without bridge piers, the t_i/H values for ice passage are smaller, while the Fr_b values are larger when bridge piers are present. The values of Fr_b and t_i/H corresponding to ice passage vary with different gate openings (e). Therefore, when analyzing whether ice floes pass through the gate, in addition to considering relevant factors such as Fr, Fr_b, Q, v, and e/H [11,21,26], the influence of e and Vol should also be taken into account.

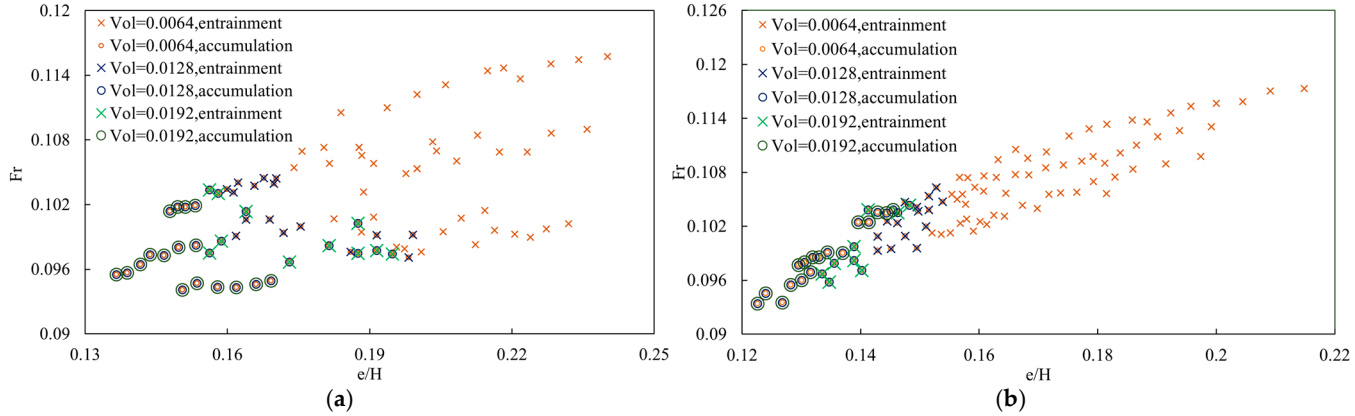


Figure 7. Scatter plot of Fr vs. e/H for different Vol without and with bridge piers ((**a**) without bridge piers; (**b**) with bridge piers).

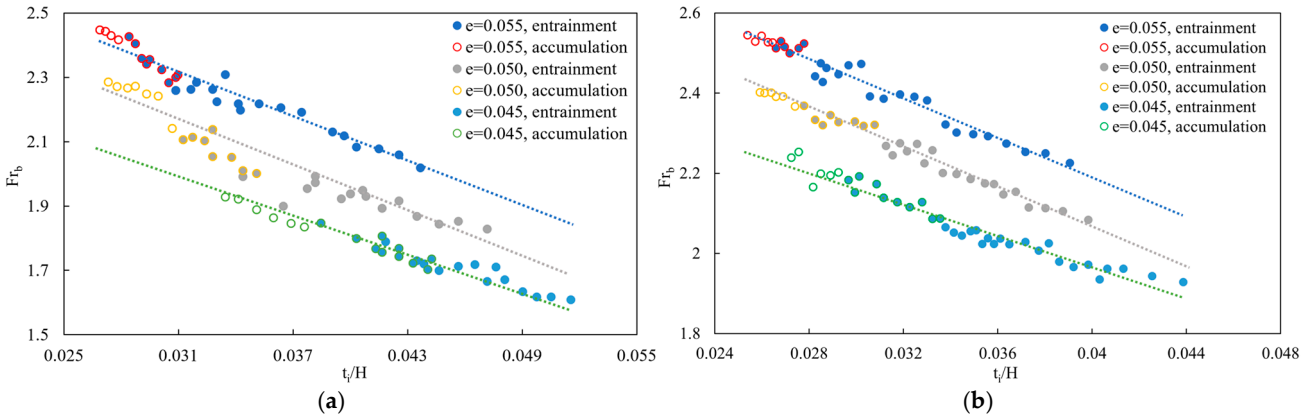


Figure 8. Scatter plot of Fr_b vs. t_i for different e without and with bridge piers ((**a**) without bridge piers; (**b**) with bridge piers).

3.2. Analysis of Correlation of Influencing Factors

To ensure the statistical validity of the experimental data and the reliability of the modeling analysis, the data suitability was first evaluated using Bartlett's test of sphericity and the Kaiser-Meyer-Olkin (KMO) statistic. The results reveal that the *p*-values of Bartlett's test for both configurations (without and with bridge piers) are less than 0.05, indicating significant inherent correlations among the influencing variables. However, the KMO statistics for the configurations without and with piers are 0.46 and 0.48, respectively. Both values fall below the acceptable threshold of 0.5 for factor analysis, demonstrating a lack of ubiquitous linear commonality among the variables. Thus, traditional linear dimensionality reduction methods, such as Principal Component Analysis (PCA) or Factor Analysis (FA), are no longer applicable. Considering that non-linear embedding techniques, such as autoencoders, are highly prone to overfitting under small sample sizes and may compromise the physical interpretability of hydraulic parameters, the SHapley Additive exPlanations (SHAP) framework—an Explainable Artificial Intelligence (XAI) approach—was introduced to replace traditional subjective feature selection methods. The calculation results are presented in Table 3 [34]. Regardless of the presence of bridge piers, the relative gate opening (e/H) and the Froude number (Fr) consistently rank as the top two most important features. In the configuration without piers, their contribution rates are 26.16% and 25.78%, respectively; in the configuration with piers, e/H and Fr still maintain a dominant influence, accounting for nearly 50% of the total importance. This indicates that the entrainment of floating ice through the gate is jointly governed by the geometric spatial constraint (e/H) and the inertial hydrodynamic drag (Fr), a fundamental mechanism that is not fundamentally altered by the presence of local structures. The introduction of bridge piers elevates the importance of discharge (Q), with its contribution rate jumping from 11.15% (without piers) to 17.62% (with piers). This is because bridge piers act as water-blocking structures, compressing the effective flow cross-section of the channel. Consequently, under the same discharge (Q), the piers induce strong localized flow acceleration and backwater effects. This makes the overall discharge (Q) a more sensitive macroscopic controlling condition for triggering ice entrainment in the vicinity of in-stream structures. In summary, despite the lack of simple linear correlations among the hydraulic parameters, whether floating ice passes through the gate is highly governed by a few macroscopic physical thresholds. This suggests that although the flow–structure–ice interaction process is exceedingly complex, the discriminant boundary determining the ultimate entrainment of the floating ice may essentially be a linear classification boundary. This relationship between the dynamic characteristics and the optimal decision boundary will be further validated through the subsequent comparison of the four machine learning models.

Table 3. SHAP values and contribution rates of variables influencing the state of floating ice under different configurations.

Variable	Without Piers		With Piers	
	SHAP	Contribution (%)	SHAP	Contribution (%)
e/H	0.142	26.155	0.165	29.938
Fr	0.140	25.777	0.109	19.602
Vol	0.099	18.176	0.097	17.521
Q	0.061	11.148	0.098	17.623
Fr_b	0.036	6.631	0.043	7.785
v	0.035	6.433	0.026	4.593
e	0.031	5.680	0.017	3.139

3.3. Comparison and Optimization of Machine Learning Models

Prior to the training and validation of the machine learning models, the experimental data were randomly divided into a training set and a testing set at a ratio of 8:2. The training set was utilized for model parameter fitting, hyperparameter tuning, and iterative optimization, while the testing set was reserved for an independent evaluation of the models' generalization and predictive capabilities, thereby ensuring the objectivity of the assessment results. To rigorously evaluate model performance and mitigate the risk of overfitting associated with small sample sizes, Stratified 5-Fold Cross-Validation was employed in this study. Table 4 quantitatively presents the evaluation metric scores and standard deviations for each model under configurations with and without bridge piers. The results indicate that, in the configuration without piers, although the SVM model achieved the highest precision with a relatively small standard deviation, its recall was only 0.77. In contrast, the LR model attained the highest levels among the four models in accuracy, recall, and the comprehensive F1 score, accompanied by small standard deviations. This demonstrates its optimal comprehensive predictive capability and high stability. Under the configuration with piers, the accuracy and F1 score of the GBDT model were slightly higher than those of the LR model; however, the standard deviations of GBDT across various metrics were noticeably larger, revealing a certain degree of instability and overfitting risk. Conversely, all performance metrics of the LR model exceeded 0.9 with smaller standard deviations, indicating more robust generalization capabilities. Figures 9 and 10 display the confusion matrices for the configurations without and with piers, respectively. Under the pier-less configuration, the false negative rate of the LR model for floating ice passing through the gate (entrainment) was 0%, whereas GBDT and RF exhibited a false negative rate of 13.3%, and SVM recorded 6.7%. In the configuration with piers, all models yielded a false negative rate of 5.9% for ice entrainment, yet the false positive rate of the LR model was significantly lower than that of the other models. Furthermore, as evidenced by the ROC curves in Figure 11, the AUC values of the LR model reached 0.993 and 0.997, respectively, demonstrating the strongest overall discriminant capability. In summary, the LR model not only boasts high computational efficiency and effectively filters out high-frequency non-linear noise from the experimental data, but also integrates high robustness, superior prediction accuracy, and strong physical interpretability across varying conditions. It perfectly fulfills the fundamental scientific research requirements for constructing explicit physical discriminant equations [35]. Therefore, this study identifies Logistic Regression (LR) as the optimal model for classifying the motion state of floating ice.

Table 4. Quantitative evaluation results of the machine learning models without and with bridge piers.

Model	Without Piers				With Piers			
	Accuracy	**Precision**	**Recall**	**F1-Score**	**Accuracy**	**Precision**	**Recall**	**F1-Score**
GBDT	0.84 (±0.06)	0.85 (±0.07)	0.80 (±0.09)	0.82 (±0.07)	0.94 (±0.04)	0.94 (±0.06)	0.90 (±0.08)	0.92 (±0.05)
RF	0.79 (±0.05)	0.80 (±0.07)	0.73 (±0.05)	0.76 (±0.05)	0.86 (±0.09)	0.89 (±0.09)	0.82 (±0.13)	0.85 (±0.10)
SVM	0.85 (±0.01)	0.90 (±0.06)	0.77 (±0.05)	0.83 (±0.01)	0.90 (±0.07)	0.94 (±0.07)	0.87 (±0.10)	0.90 (±0.07)
LR	0.88 (±0.02)	0.87 (±0.05)	0.89 (±0.04)	0.87 (±0.03)	0.92 (±0.02)	0.94 (±0.03)	0.90 (±0.06)	0.91 (±0.03)

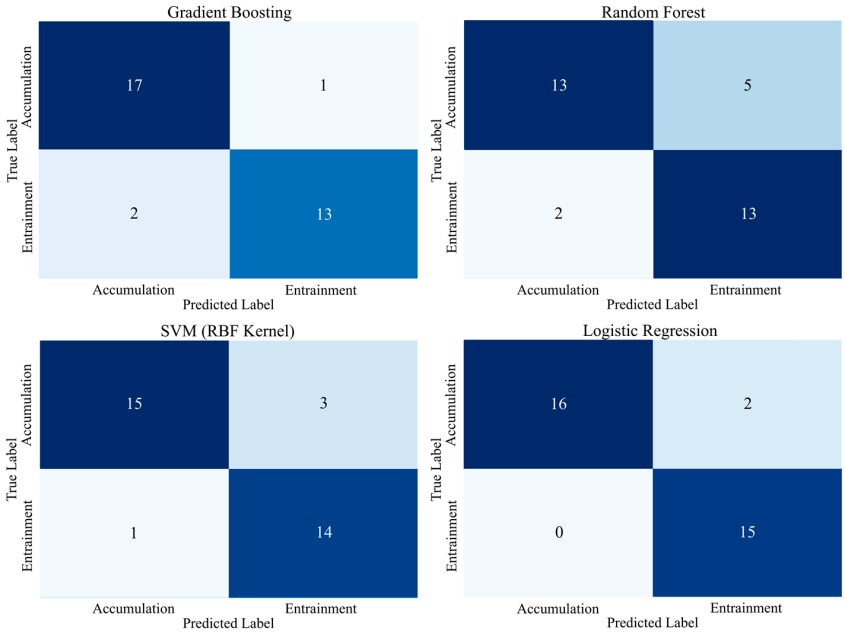


Figure 9. Confusion matrices of models without bridge piers.

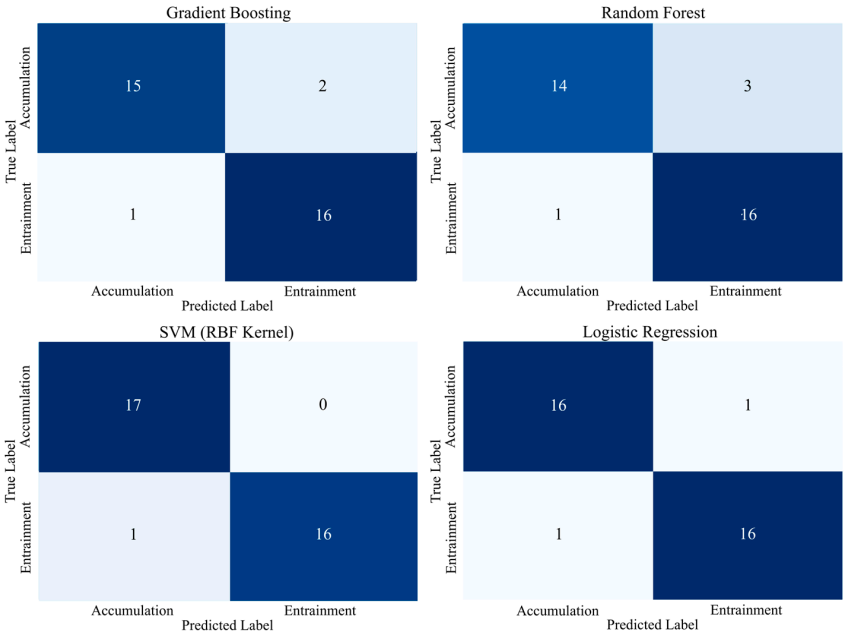


Figure 10. Confusion matrices of models with bridge piers.

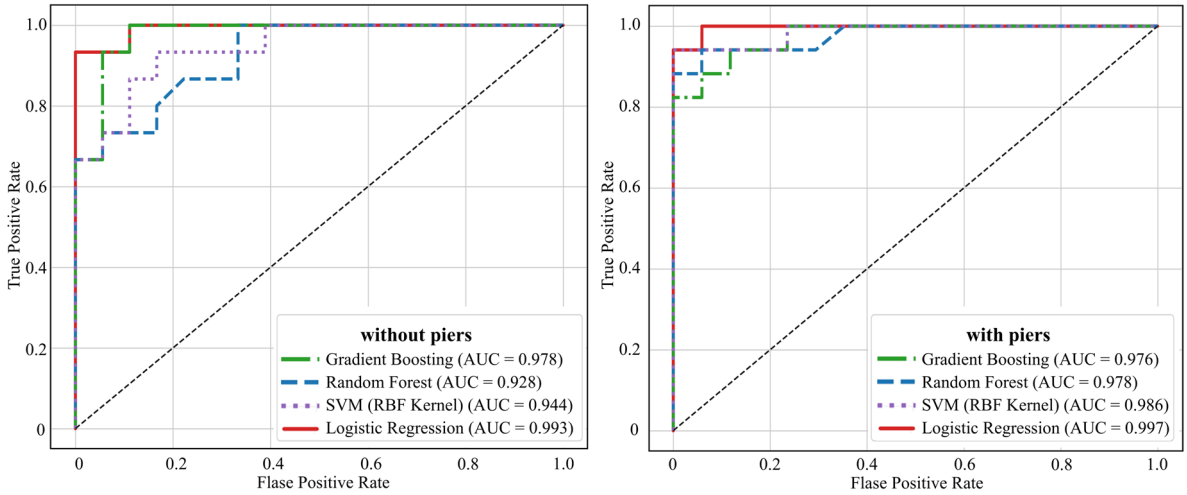


Figure 11. ROC curves of models without and with bridge piers.

3.4. Construction of the Ice Floe Entrainment Model Based on Logistic Regression (LR)

Based on the input of all variables, the LR model exhibited optimal classification performance. By analyzing its decision boundaries and applying Z-score standardization, initial discriminant formulas incorporating seven influencing parameters were derived for conditions with and without bridge piers. The expression of the Sigmoid function representing the probability of ice floes passing through the sluice gate is shown in Equation (5):

$$P = \frac{1}{1 + e^{-Z}} \tag{5}$$

where, when $Z > 0$ ($p > 0.5$), it is determined that ice floes pass through the sluice gate; when $Z < 0$ ($p < 0.5$), it is determined that ice floes accumulate upstream of the gate. To eliminate dimensional discrepancies and accurately quantify the contribution weight of each parameter, Z-score standardization was applied to each independent variable. The fitting results of the linear discriminant function Z for conditions without and with bridge piers are presented in Equations (6) and (7), respectively:

Without bridge piers:

$$Z = -0.16 + 1.79 \times e_{std} - 1.09 \times Q_{std} - 0.03 \times v_{std} + 1.76 \times (e/H)_{std} + 1.20 \times Vol_{std} - 0.94 \times (Fr_b)_{std} + 1.63 \times Fr_{std} \tag{6}$$

With bridge piers:

$$Z = 0.79 + 0.82 \times e_{std} - 1.71 \times Q_{std} - 0.18 \times v_{std} + 2.16 \times (e/H)_{std} + 1.53 \times Vol_{std} - 0.81 \times (Fr_b)_{std} + 1.99 \times Fr_{std} \tag{7}$$

In Equations (6) and (7), a positive regression coefficient facilitates the entrainment of floating ice through the sluice gate; the larger the absolute value of the coefficient, the higher the probability of the floating ice passing through the sluice gate. Conversely, a negative coefficient exerts an inhibitory effect; the larger its absolute value, the more prone the floating ice is to accumulate upstream of the gate. Although the full-variable model exhibits excellent statistical fitting accuracy, considering that variables such as v, Q, and Fr essentially represent the identical hydrodynamic process, parameter redundancy can easily trigger risks of multicollinearity, thereby weakening the physical interpretability of the model [36]. Based on the SHAP values and contribution rates of each influencing variable in Table 3, it is evident that regardless of the presence of bridge piers, the SHAP contribution rates of Fr, e/H, and Vol to the model predictions consistently rank at the forefront. In contrast, the contribution rates of v, e, and Fr_b are relatively low. Furthermore,

Figure 12 presents the Pearson correlation heatmaps for the configurations with and without piers. As indicated by the quantitative correlation coefficients in the figure, under both configurations, the correlation coefficients among v, Q, and Fr_b all exceed 0.8, exhibiting strong positive correlation clustering. This indicates that the information carried by v and Q can be effectively encompassed by Fr, the core hydrodynamic factor within the same dimension, confirming the existence of parameter redundancy. Integrating the SHAP feature importance rankings from Table 3, and given that Fr and e/H exhibit the highest global contribution rates, this study eliminated redundant parameters such as v, Q, and Fr_b. Instead, only three core factors were retained for the simplified variable modeling: Fr (representing the hydrodynamic drive), e/H (representing the geometric constraint), and Vol (representing the characteristics of the floating ice). To further enhance the universal applicability of the formula, Vol was non-dimensionalized as follows:

$$\phi = \frac{Vol}{L \times B \times H} \tag{8}$$

where ϕ represents the dimensionless ice volume concentration; L is the distance from the ice release point to the gate; and B is the flume width.

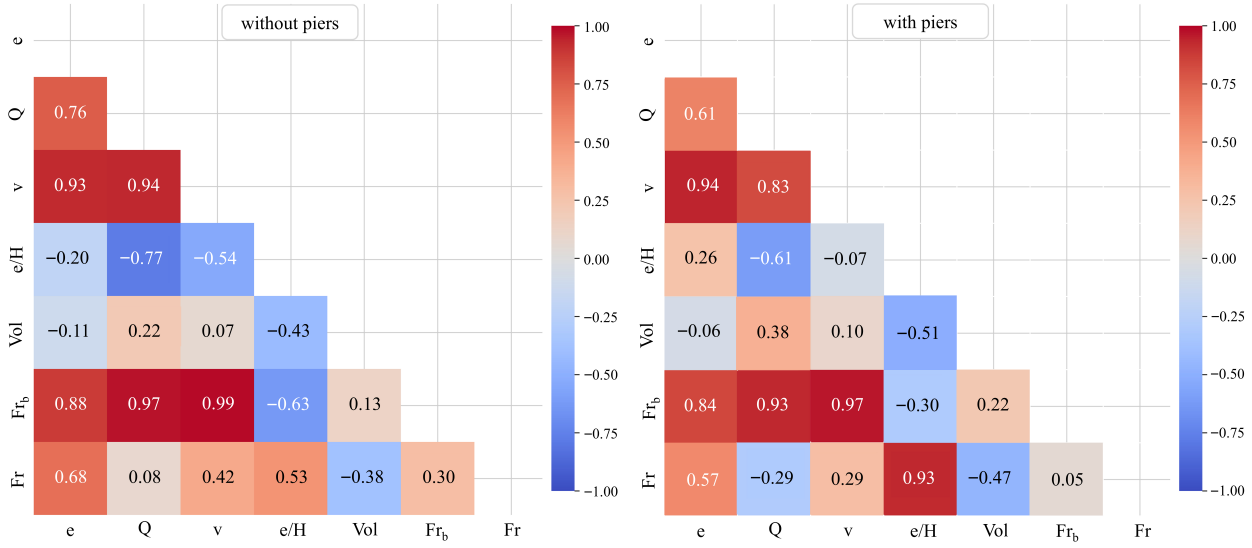


Figure 12. Pearson correlation heatmaps for configurations without and with bridge piers.

To diagnose the risk of multicollinearity among the core variables, the Variance Inflation Factor (VIF) was employed to test Fr, e/H, and ϕ under both conditions. The results are shown in Table 5. In the absence of bridge piers, the VIF values for Fr, e/H, and ϕ were all below the multicollinearity threshold of 5, indicating no significant linear correlation. In the presence of bridge piers, the VIF values for Fr and e/H increased to 7.27 and 7.69, respectively, indicating slight multicollinearity; however, this does not affect the description of the core physical mechanism [37].

Table 5. VIF results for three variables without and with bridge piers.

Conditions	*Fr*	*e/H*	*ϕ*
without piers	1.45	1.52	1.27
with piers	7.27	7.69	1.35

After adopting the dimensionless factor, the final fitting results of the linear discriminant function are shown in Equations (9) and (10):

Without bridge piers:

$$Z = -0.06 + 1.95 \times (e/H)_{std} + 2.17 \times Fr_{std} + 1.01 \times \phi_{std} \quad (9)$$

With bridge piers:

$$Z = 0.51 + 4.02 \times (e/H)_{std} + 0.32 \times Fr_{std} + 1.24 \times \phi_{std} \quad (10)$$

Table 6 presents the quantitative evaluation results of the LR model after simplifying the input variables for both pier configurations. Compared to Table 4, although the performance of the reduced-variable model exhibits a marginal decline, it overall remains within an excellent range. Specifically, the confusion matrices in Figure 13 reveal that under the configuration without piers, there are only 2 false negatives (missed entrainment samples) and 1 false positive (misclassified accumulation sample). Under the configuration with piers, the numbers of both false positives and false negatives are strictly controlled to within 3. This demonstrates a high level of classification sensitivity and specificity. Furthermore, the ROC curves in Figure 14 indicate that the AUC values for the configurations without and with piers are 0.989 and 0.952, respectively, both closely approaching the ideal value of 1.0. Collectively, these results demonstrate that the feature selection process effectively eliminated redundant noise induced by multicollinearity while integrally preserving the core physical mechanisms. Consequently, the LR model is still able to precisely capture the non-linear decision boundary governing the entrainment of floating ice through the gate under complex flow conditions, thereby maintaining exceptional classification efficacy.

Table 6. Quantitative evaluation results of the Logistic Regression model without and with bridge piers after variable simplification.

Conditions	Accuracy	Precision	Recall	F1-Score
without piers	0.85 (±0.04)	0.86 (±0.08)	0.83 (±0.05)	0.84 (±0.03)
with piers	0.91 (±0.04)	0.92 (±0.03)	0.90 (±0.08)	0.91 (±0.05)

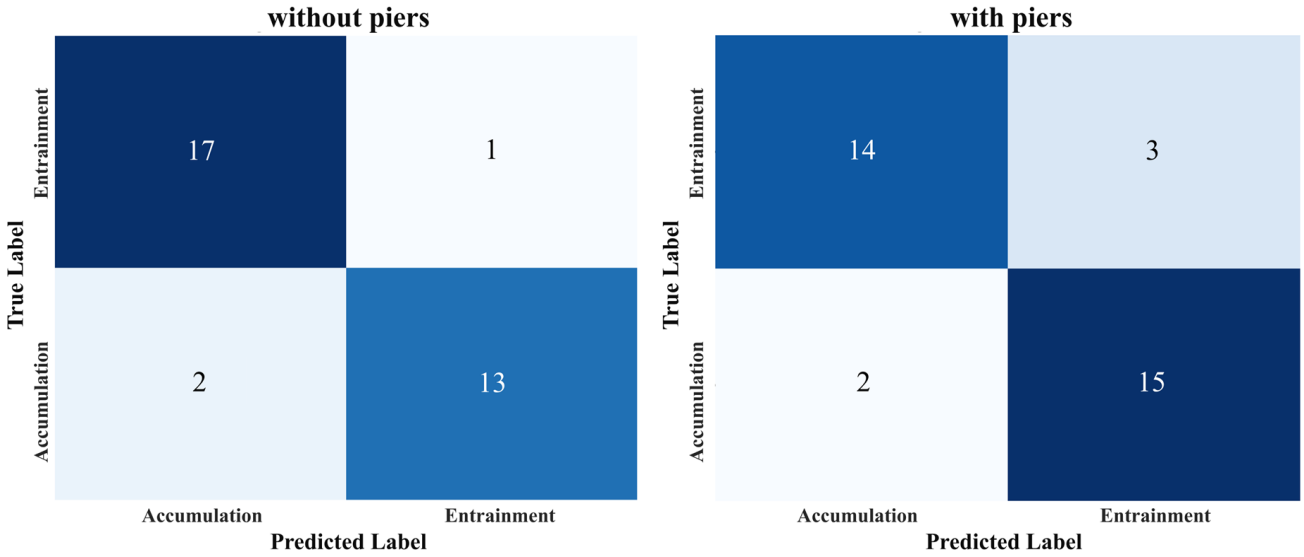


Figure 13. Confusion matrices of the LR model without and with bridge piers.

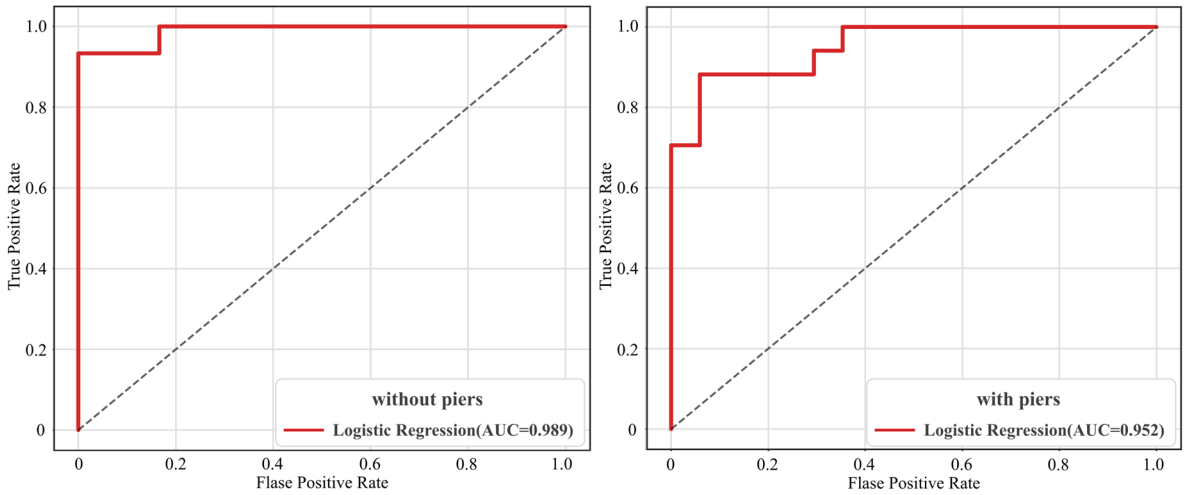


Figure 14. ROC curves of the LR model without and with bridge piers.

4. Discussion

4.1. Relative Contribution Weights of Core Parameters and Multi-Dimensional Clustering Features

The magnitude of the standardized regression coefficients intuitively quantifies the relative contribution weight of each core dimensionless term to the process of ice floe entrainment. As indicated by Equations (9) and (10), under the condition without bridge piers, the standardized regression coefficients of e/H and Fr are slightly higher than that of ϕ. This suggests that in this scenario, ice floe entrainment is synergistically dominated by the geometric constraint e/H and the hydrodynamic intensity Fr, while the promoting effect of ice concentration ϕ is relatively weak. In contrast, under the condition with bridge piers, the standardized regression coefficient of e/H is significantly higher than those of Fr and ϕ. This indicates that the presence of bridge piers amplifies the regulatory effect of the relative gate opening on the local flow field, further reinforcing the controlling status of e/H. Meanwhile, the contribution of hydrodynamic intensity characterized by Fr is attenuated due to flow field distortion, resulting in a significant reduction in its influence weight.

To intuitively reveal the data distribution structures and clustering characteristics of the core variables in a multidimensional space, Figure 15 presents the paired scatterplot matrices of the core variables for the two motion states of floating ice under configurations with and without bridge piers. Observing the Kernel Density Estimation (KDE) curves on the diagonal, it is evident that the accumulation and entrainment states of the floating ice exhibit distinct data cluster separation across all single dimensions. Particularly in the e/H dimension, the probability density peaks of the two sample categories are significantly offset: the samples in the accumulation state are highly concentrated in the low-opening range, whereas the samples in the entrainment state (passing through the gate) shift toward the high-opening range. The minimal overlap area under their KDE curves preliminarily demonstrates the exceptionally high classification discrimination of this variable. In the off-diagonal two-dimensional projection spaces, the clustering characteristics of the samples are further accentuated. Without bridge piers, although the scatter plots of Fr and e/H show partial overlap between the accumulation and entrainment regions, the overall discrimination remains robust. However, when ϕ is coupled with other core parameters, the scatter overlap is higher, indicating that e/H and Fr are the core driving factors under this configuration. With bridge piers, in the scatter plots where e/H is coupled with other core parameters, the entrainment conditions (red dots) are distinctly concentrated in regions with higher values. The discrimination from the accumulation conditions (blue dots) is notably higher than that in the pier-less configuration. This indicates that the flow field

interference induced by the piers renders e/H the critical parameter for distinguishing the state of the floating ice, significantly elevating its regulatory priority.

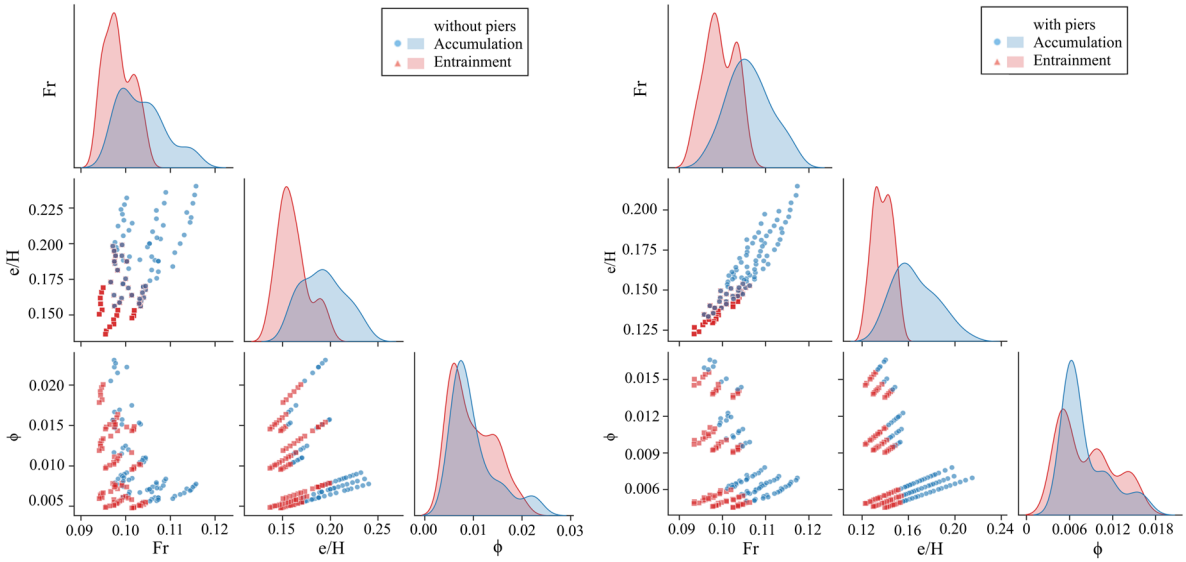


Figure 15. Scatter plot matrix of paired variables without and with bridge piers.

4.2. Determination of Engineering Critical Thresholds

To provide a directly quantifiable operational basis for ice period scheduling in hydraulic engineering in cold regions, this study derived critical equilibrium constraint equations for the original physical parameters under conditions with and without bridge piers, based on the critical decision boundary (p = 0.5, i.e., Z = 0) of the LR discriminant model. Through the inverse transformation process of Z-score standardization and by substituting the statistical characteristic values of the experimental data, the critical constraint equations for both conditions were obtained. The formula without bridge piers is:

$$e/H = 0.77 - 5.60Fr - 2.84\phi \quad (11)$$

The formula with bridge piers is:

$$e/H = 0.19 - 0.29Fr - 1.79\phi \quad (12)$$

Equations (11) and (12) establish the synergistic constraint relationships that e/H and Fr must satisfy at the critical state of floating ice entrainment or accumulation. These equations are derived from the standardized model Formulas (9) and (10) through a rigorous linear inverse transformation. They maintain mathematical equivalence with the original model, thereby ensuring that the prediction accuracy of the critical thresholds is consistent with the preceding model. By substituting the dimensionless mean values of the experimental data into the calculation, the critical safety thresholds for typical conditions can be obtained: the critical relative gate opening (e/H) without bridge piers is 0.176, whereas this value decreases to 0.149 with bridge piers. However, considering the inevitable measurement disturbances in hydraulic model experiments and the profound randomness inherent in natural ice transport processes, providing a single deterministic threshold is insufficient to comprehensively reflect the risk intervals in practical engineering. To address this, the Bootstrap resampling technique is introduced in this study to conduct an in-depth quantitative assessment of the uncertainty associated with the critical thresholds. Figure 16 presents the frequency distribution of the e/H critical thresholds calculated through 1000 Bootstrap resampling iterations. The results indicate that the critical

threshold is not an isolated absolute value but follows an approximately normal probability distribution. At a 95% confidence level, the probability interval of the threshold for the configuration without piers lies between [0.170, 0.182], whereas for the configuration with piers, it is distributed between [0.142, 0.155]. The presence of bridge piers compresses the safe operational margin for gate dispatch during the ice period by approximately 15%. Therefore, a more conservative gate opening strategy must be adopted in scenarios with bridge piers to avert the risk of floating ice passing through the gate. This probabilistic range, featuring explicit confidence intervals, not only quantitatively reveals the fluctuation boundaries of the critical state but also provides a more flexible decision-making space for practical water conveyance projects in cold regions. In winter ice-prevention dispatching, operators can designate the lower limit of the 95% confidence interval as a conservative extreme warning baseline, thereby significantly enhancing the operational reliability of the sluice gate.

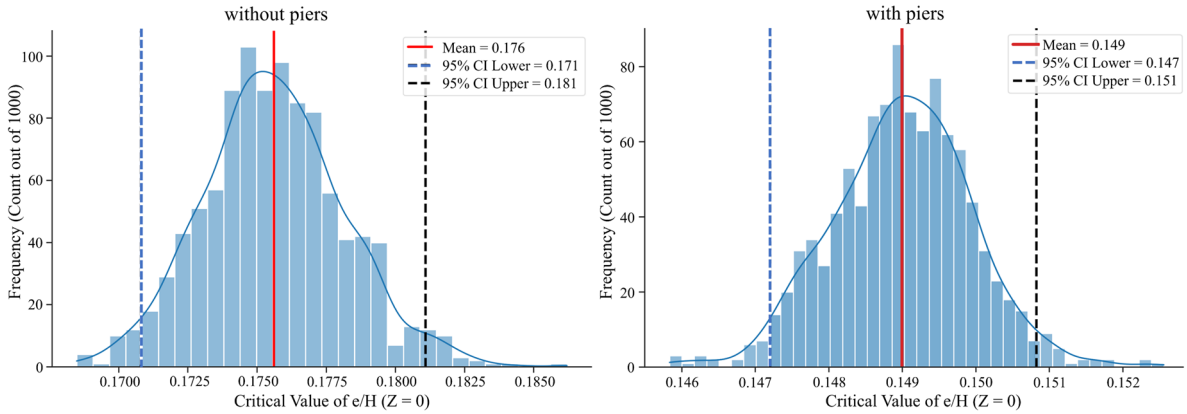


Figure 16. Bootstrap uncertainty distribution of the critical threshold *e/H* for floating ice entrainment.

4.3. Transferability and Potential Value of the Results

Among the multi-dimensional hydraulic parameters initially selected in this study, the SHAP value analysis clarified the hierarchy of physical driving forces controlling floating ice entrainment. Regardless of the presence of bridge piers, the dimensionless parameters—relative gate opening (e/H) and Froude number (Fr)—consistently occupied dominant positions, with a cumulative contribution rate ranging from 45.37% to 51.93%. This feature composition, dominated by dimensionless parameters, proves that the core mechanism of ice entrainment follows hydraulic similarity criteria, thereby transcending the geometric scale limitations of flume models. Simultaneously, analysis results from the multi-dimensional scatter matrix and Kernel Density Estimation (KDE) demonstrate that the two motion states—ice accumulation and entrainment—exhibit distinct probability density peak offsets in the e/H dimension with low regional overlap, indicating that e/H is a highly stable classification feature. Consequently, when applying this framework to other cold-region hydraulic structures such as canals or spillways, engineers only need to combine local field observation data to locally recalibrate the coefficients of the explicit equations, enabling the derivation of high-precision discrimination thresholds adapted to new scenarios across different scales. The data analysis results of standardized regression coefficients and critical threshold intervals within the feature discrimination framework constructed in this study corroborate each other, revealing the risk amplification effect of bridge piers on floating ice entrainment. Data indicate that the presence of piers disrupts the local flow field and significantly increases the influence weight of e/H, leading to a reduction and compression of the critical e/H threshold interval from [0.170, 0.182] without piers to [0.142, 0.155] with piers. This numerical variation pattern provides a crucial

quantitative design basis for safety margin reservation in coupled gate–pier hubs. During actual ice-jam season operations, flood control departments can embed the proposed explicit critical equations—after parameter calibration—into hydraulic Digital Twin or SCADA dispatching systems to prevent physical impact damage to the gate sill and key downstream facilities caused by large-scale ice entrainment.

5. Conclusions

This study employed a combined approach of physical model tests and machine learning to systematically investigate the core mechanisms governing the motion states of ice floes upstream of the sluice gate, as well as the critical thresholds for entrainment, under conditions without and with bridge piers. The main conclusions are as follows:

(1) Influenced by factors such as incoming hydraulic parameters, gate boundary conditions, and incoming ice volume, the motion state of ice floes upstream of the gate exhibits a developmental progression of "flat accumulation → "∇"-shaped accumulation → wedge-shaped accumulation → entrainment (passage through the gate)."

(2) Compared to the GBDT, RF, and SVM models, the LR model achieves higher and more stable accuracy, precision, recall, and F1 scores under configurations without and with bridge piers. With AUC values reaching 0.993 and 0.997, respectively, this model demonstrates optimal comprehensive performance in classifying whether floating ice passes through the gate.

(3) Based on the LR model, discriminant formulas for the critical thresholds of ice entrainment with and without bridge piers were constructed. Under the specific experimental conditions herein, the critical threshold ranges of e/H without and with bridge piers are [0.170, 0.182] and [0.142, 0.155], respectively.

This study supplements the multi-parameter synergistic mechanisms underlying ice transport, accumulation, and entrainment upstream of the gate. It refines the theoretical framework of flow–structure–ice interactions during the ice period and provides quantitative thresholds and adaptive methods, thereby offering a calculative framework for winter gate dispatching in hydraulic projects. However, as a fundamental generalized physical flume experiment, this study still possesses certain limitations that warrant further in-depth investigation in future work. The experimental conditions have not yet accounted for the influence of complex factors such as the number and morphology of bridge piers, the heterogeneity of ice size and thickness, and concurrent riverbed scour. In an authentic, complex hydraulic environment, the critical safety thresholds will experience dynamic shifts. Nevertheless, the baseline rules and machine learning prediction framework established under controlled conditions in this study lay a crucial methodological foundation for coupling the aforementioned complex boundaries in future research. From the perspective of comprehensive engineering flood and ice defense, although restricting the entrainment of floating ice through the gate can guarantee structural safety, causing massive ice accumulation upstream of the gate will lead to a sharp reduction in the effective flow cross-section and elevated upstream water levels, potentially triggering ice jam floods. Future research may consider integrating the coupled gate–pier structure with auxiliary facilities such as ice booms to guide the floating ice to form a stable ice cover in safe areas, thereby achieving safe water conveyance beneath the ice. Furthermore, the discriminant criteria and critical thresholds proposed herein were derived based on the flume experimental data of this study, which cover a Froude number (Fr) range of 0.09 to 0.12, without considering high-discharge conditions or climate-driven ice regime evolution. When extrapolating this threshold system to actual large-scale water conservancy hubs or natural rivers, the impacts of scale effects must be carefully considered. Future studies could expand the range of experimental conditions and combine large-scale physical model experiments or

high-fidelity 3D numerical simulations to calibrate and modify the proposed critical equations at the prototype scale, thereby further guiding ice-prevention dispatching practices in cold region engineering.

Author Contributions: Conceptualization, S.L. and C.L.; methodology, S.L. and C.L.; software, S.L., H.H. and S.Z.; validation, S.L. and C.L.; investigation, H.H. and X.L.; data curation, S.L.; writing—original draft preparation, S.L., C.L. and S.Z.; writing—review and editing, S.L. and C.L.; supervision, H.H. and X.L.; funding acquisition, C.L. All authors have read and agreed to the published version of the manuscript.

Funding: This research was funded by the National Natural Science Foundation of China—Yellow River Water Science Joint Fund (grant No. U2443205), the Inner Mongolia Autonomous Region Science and Technology Plan Project (grant No. 2023YFSH0002), the Natural Foundation of Inner Mongolia (grant No. 2023MS05023), the Central Government Guided Local Science and Technology Development Fund Project (grant No. 2024ZY0065), and the Basic Scientific Research Business Fee of Directly affiliated Universities in Inner Mongolia Autonomous Region (grant No. BR231516).

Data Availability Statement: The data presented in this study are available in the article.

Acknowledgments: Acknowledgements are extended to the State Key Laboratory of Water Engineering Ecology and Environment in Arid Area, Inner Mongolia Agricultural University for their financial support of this research paper.

Conflicts of Interest: The authors declare no conflicts of interest.

References

1. Donnelly, J.; Daneshkhah, A.; Abolfathi, S. Physics-informed neural networks as surrogate models of hydrodynamic simulators. *Sci. Total Environ.* **2024**, *912*, 168814. [CrossRef]
2. Tang, Y.; Feng, J.; Wang, J.; Sui, J.; Li, G. Research on the mechanical equilibrium equation of ice jam. *J. Hydrodyn.* **2025**, *37*, 320–330. [CrossRef]
3. Shen, H.T. River ice processes–half-century of research progress. *J. Hydraul. Res.* **2025**, *64*, 3–17. [CrossRef]
4. Zhang, M.; Qu, X.; Kalhori, H.; Ye, L. Indirect monitoring of distributed ice loads on a steel gate in a cold region. *Cold Reg. Sci. Technol.* **2018**, *151*, 267–287. [CrossRef]
5. Dong, S.; Zhang, Z.; Li, Z.; Chen, P.; Wang, J.; Li, G. Analysis of Local Scour around Double Piers in Tandem Arrangement in an S-Shaped Channel under Ice-Jammed Flow Conditions. *Water* **2024**, *16*, 2831. [CrossRef]
6. Ashton, G.D. Froude Criterion for Ice-Block Stability. *J. Glaciol.* **1974**, *13*, 307–313. [CrossRef] [PubMed]
7. Ashton, G.D. Ice entrainment through submerged gate. In Proceedings of the 19th IAHR International Symposium on Ice, Vancouver, BC, Canada, 6–11 July 2008; pp. 179–188.
8. Zheng, Y.; Mu, X.; Wen, H. Water Ability Research of Flat Gate Under the Conditions of the Ice Cover. *Yellow River* **2012**, *34*, 142–143. [CrossRef]
9. Zheng, Y.; Mu, X.; Ji, H.; Zhao, M.; Wang, L. Research on Accumulation Morphology of Ice in Front of Sluice Under the Condition of Outflow from Sluice Opening. *Yellow River* **2020**, *42*, 27–31+36. [CrossRef]
10. Fu, H.; Yang, K.; Guo, X.; Guo, Y.; Wang, T. Safe operation of inverted siphon during ice period. *J. Hydrodyn.* **2015**, *27*, 204–209. [CrossRef]
11. Fu, H.; Guo, X.; Yang, K.; Wang, T.; Guo, Y. Ice accumulation and thickness distribution before inverted siphon. *J. Hydrodyn.* **2017**, *29*, 61–67. [CrossRef]
12. Wang, J.; Hou, Z.; Sui, J.; Cheng, T. Advances in research work regarding impacts of bridge piers on ice accumulation and local scour processes. *Chin. J. Theor. Appl. Mech.* **2021**, *53*, 672–681. [CrossRef]
13. Wu, Y.; Zhu, M.; Mu, X.; Yue, C.; Zhou, F. Study on ice-passing capacity of pier-column section in channel. *Water Resour. Hydropower Eng.* **2017**, *48*, 126–131. [CrossRef]
14. Mu, X.; Bao, J.; Chen, Y. Floating ice transport conditions at the cross-sections between pier columns in open ice-water two-phase flow canals. *Water* **2020**, *12*, 1813. [CrossRef]
15. Wang, J.; Shi, F.; Chen, P.; Wu, P.; Sui, J. Impacts of bridge piers on the initiation of ice cover—An experimental study. *J. Hydrol. Hydromech.* **2015**, *63*, 327. [CrossRef]
16. Wang, J.; Hua, J.; Sui, J.; Wu, P.; Liu, T.; Chen, P. The impact of bridge pier on ice jam evolution—An experimental study. *J. Hydrol. Hydromech.* **2016**, *64*, 75. [CrossRef]

17. Wang, J.; Hua, J.; Chen, P.; Sui, J.; Wu, P.; Whitcombe, T. Initiation of ice jam in front of bridge piers—An experimental study. *J. Hydrodyn.* **2019**, *31*, 117–123. [CrossRef]
18. Hu, H.; Wang, J.; Cheng, T.; Hou, Z.; Sui, J. Channel bed deformation and ice jam evolution around bridge piers. *Water* **2022**, *14*, 1766. [CrossRef]
19. Cheng, T.; Wang, J.; Chen, P.; Sui, J. Simulation of ice accumulation around bridge piers during river breakup periods using a discrete element model. *J. Hydrodyn.* **2022**, *34*, 94–105. [CrossRef]
20. Karami, S.; Heidari, M.M.; Rad, M.H.A. Investigation of free flow under the sluice gate with the sill using flow-3D model. *Iran. J. Sci. Technol. Trans. Civ. Eng.* **2020**, *44*, 317–324. [CrossRef]
21. Norouzi, R.; Ebadzadeh, P.; Sume, V.; Daneshfaraz, R. Upstream vortices of a sluice gate: An experimental and numerical study. *AQUA—Water Infrastruct. Ecosyst. Soc.* **2023**, *72*, 1906–1919. [CrossRef]
22. Rady, R.A.E.H. Modeling of flow characteristics beneath vertical and inclined sluice gates using artificial neural networks. *Ain Shams Eng. J.* **2016**, *7*, 917–924. [CrossRef]
23. Hassanzadeh, Y.; Abbaszadeh, H. Investigating discharge coefficient of slide gate-sill combination using expert soft computing models. *J. Hydraul. Struct.* **2023**, *9*, 63–80. [CrossRef]
24. Cao, D.; Li, G.; Li, S. Analysis of Hydraulic Characteristics of Submerged Gate Discharge Based on Hybrid Artificial Intelligence Models. *Flow Meas. Instrum.* **2025**, *108*, 103155. [CrossRef]
25. Liang, N.; Tuo, Y.; Deng, Y.; Jia, Y. Classification Model of Ice Transport and Accumulation in Front of Channel Flat Sluice Based on PCA-SVM. *Chin. J. Theor. Appl. Mech.* **2021**, *53*, 703–713. [CrossRef]
26. Liang, N.; Tuo, Y.; Deng, Y.; He, T. PCA-based SVM classification for simulated ice floes in front of sluice gates. *Polar Sci.* **2022**, *34*, 100839. [CrossRef]
27. Li, Z.; Wang, J.; Sui, J.; Cheng, T.; Liu, P.; Li, G. Channel bed deformation around double piers in tandem arrangement in an S-shaped channel under ice cover. *Water* **2023**, *15*, 2568. [CrossRef]
28. Li, Z.; Zhang, Z.; Sui, J.; Wang, J. Experimental Assessment of Scour Around Side-by-Side Double Piers in an S-Shaped Channel with Ice-Jammed Flow. *Water* **2025**, *17*, 1768. [CrossRef]
29. Hu, L.; Zhou, Y. Study on Automatic Flow Measurement in Rectangular Open Channel Based on Dilution Method. *Water Sav. Irrig.* **2020**, *7*, 85–88.
30. Nejatipour, P.; Oliveto, G.; Sapaev, I.; Afaridegan, E.; Fatahi-Alkouhi, R. Prediction and Uncertainty Quantification of Flow Rate Through Rectangular Top-Hinged Gate Using Hybrid Gradient Boosting Models. *Water* **2025**, *17*, 3470. [CrossRef]
31. Baalousha, H.M. Machine Learning-Driven Calibration of Modflow Models: Comparing Random Forest and XGBoost Approaches. *Geosciences* **2025**, *15*, 303. [CrossRef]
32. Bagherzadeh, S.; Ghaeini-Hessaroeyeh, M.; Fadaei-Kermani, E. Prediction of cavitation damage using SVM model based on air–water two-phase flow over dam spillway. *Appl. Water Sci.* **2025**, *15*, 70. [CrossRef]
33. Gad, M.; Marie, H.S.; Abozaid, G.M. Employing artificial intelligence to improve the accuracy of hydraulic jump length predictions in water engineering. *Water Resour. Manag.* **2025**, *39*, 4071–4092. [CrossRef]
34. Basumatary, M.; Maji, S.; Kumar, B. SHAP-based interpretation of machine learning models in bed load transport prediction. *Model. Earth Syst. Environ.* **2026**, *12*, 65. [CrossRef]
35. Maniatis, G.; Hoey, T.B.; Hassan, M.A.; Sventek, J.; Hodge, R.; Drysdale, T.; Valyrakis, M. Calculating the explicit probability of entrainment based on inertial acceleration measurements. *J. Hydraul. Eng.* **2017**, *143*, 04017004. [CrossRef]
36. Zhu, Y.; Zheng, Y.; Yin, M. Multicollinearity Test Under Statistical Significance. *Stat. Decis.* **2020**, *36*, 34–36. [CrossRef]
37. Cole, D.J.; Morgan, B.J.T. Parameter redundancy with covariates. *Biometrika* **2010**, *97*, 1002–1005. [CrossRef]

Disclaimer/Publisher's Note: The statements, opinions and data contained in all publications are solely those of the individual author(s) and contributor(s) and not of MDPI and/or the editor(s). MDPI and/or the editor(s) disclaim responsibility for any injury to people or property resulting from any ideas, methods, instructions or products referred to in the content.